

Article

Structure of Highly Porous Silicon Dioxide Thin Film: Results of Atomistic Simulation

F.V. Grigoriev *, V.B. Sulimov and A.V. Tikhonravov

Research Computing Center, M. V. Lomonosov Moscow State University, 119991 Moscow, Russia

* Correspondence: fedor.grigoriev@srcc.msu.ru

Received: 5 August 2019; Accepted: 2 September 2019; Published: 5 September 2019



Abstract: The high-energy glancing angle deposition of silicon dioxide films with alternation of deposition angle is studied using classical atomistic simulation. Both slow and fast alternations are investigated. The growth of vertical tree-like columns and chevron-like regular structures is demonstrated under fast and slow alternations, respectively. Due to high porosity, the density of the deposited silicon dioxide films is reduced to $1.3 \div 1.4 \text{ g/cm}^3$. This results in reduction of the refractive index to 1.3, which agrees with known experimental data. For slow continuous substrate rotation, formation of a helical structure is demonstrated.

Keywords: thin films; glancing angle deposition; refractive index; highly porous films

1. Introduction

Glancing angle deposition (GLAD) [1] is a promising technique for producing films with reduced refractive index and anisotropic properties [2]. Unlike normal deposition, in the GLAD technique, deposited particles move almost parallel to the substrate, which results in the formation of separate nanostructures [2]. The shape and size of these nanostructures depend on the deposition angle between the normal to the substrate and the direction of velocity of the deposited particles. The increase in deposition angle results in growth of film porosity and reduction of the film refractive index [1,2].

GLAD films are used in linear polarizers [3], liquid crystal displays as alignment layers [4], optical coatings with low reflectance [5], and anti-reflection coatings for high power lasers [6]. GLAD, with alternation of deposition angle, ensures the fabrication of thin films for polarization rotators [7], birefringent reflectors [8], and other optical devices requiring films with anisotropic properties and low refractive indexes.

For simulation of the GLAD films' growth, a ballistic model with Monte Carlo sampling has been widely used (see [9–12] and also multiple references in these publications). In [11], a 3D-ballistic simulator was applied to model the growth and morphology of GLAD films. It was revealed that the density of these films, normalized to the density of the typically deposited films, is approximately 0.4. The reason for low density of the GLAD films is the formation of isolated microcolumns in their internal structure [11]. In [12], 3D ballistic simulation was applied to study self-shadowing and growth competition in the formation of GLAD film nanostructures. The model predicting the dependence of the angle between the columnar structures and the normal to the substrate (tilt angle) on the deposition conditions has been developed. The classical molecular dynamics (MD) method is used in [13] for simulation of a titanium film deposition. The number of deposited atoms was $\sim 10^4$. A coincidence was found in the calculated and experimental values of the saturated roughness exponent. In [14], growth of a TiO_2 thin film is simulated using the MD and kinetic Monte Carlo methods. The formation of a slanted columnar structure is demonstrated for CLAD. The dependence of the main components of the anisotropic refractive index on the deposition conditions of GLAD-films is investigated using the anisotropic Bruggeman effective medium theory for many-component materials [15].

The earlier-developed full-atomistic method [16–18], based on classical molecular dynamics (MD), was applied to the study of GLAD SiO₂ films in [19]. The formation of slanted columnar structures under different deposition conditions was also investigated in [19].

The main goal of this paper is to demonstrate that, at the current level of mathematical modeling, atomistic simulation of the deposition process becomes a reliable tool to predict the structural properties of GLAD films. We take into consideration the high-energy GLAD silicon dioxide films obtained with alternation of deposition angle. They are investigated using the simulation method developed in [16–19]. Film deposition is simulated for cases of slow and fast alternations in the direction of flow of deposited particles. The simulation results are compared with experimental data.

2. Method

The film deposition process is simulated using an MD-based step-by-step procedure, as described in [16–18]. Clusters of the silica glass substrate are prepared by the melting-quenching method from an alpha-quartz crystal, as described in [16]. Horizontal dimensions of the small and large substrate clusters are 10 nm × 30 nm and 20 nm × 60 nm, respectively. The vertical dimension of both substrate clusters was kept at 6 nm. The empirical pairs-wise DESIL force field [20] is used for calculation of interatomic energy. It has been proven that the force field provides reliable reproduction of structural and mechanical properties of silica dioxide films deposited under different conditions [20].

At each injection step, silicon and oxygen atoms with stoichiometric proportion of 1:2 are inserted randomly at the top of the simulation box. The total number of silicon and oxygen atoms directed to the substrate per injection step is equal to 180 and 720 for small and large substrate clusters, respectively. This ensures the same flux density of deposited atoms as in previous works [16–19]. In this work, flux density was chosen so as to provide an optimal correlation between simulation time and accurate calculation of the relaxation processes caused by the deposited atoms. The initial values of the silicon and oxygen atoms' velocities correspond to the deposited atoms' kinetic energy. The experimental distribution of the sputtered atoms kinetic energy is described by Thomson formula [21] with the maximum being equal to half of the surface binding energy, which is approximately 2.5 eV for the case of the silicon target. Our previous simulations [19] revealed that the structure of GLAD films varies significantly when the energy of sputtered silicon atoms increases from 1.0 to 10 eV. In this work, we focus our attention on studying how high-energy sputtered atoms effect film structures. For this reason, the kinetic energy of silicon atoms is chosen as 10 eV. This value takes into account the high-energy part of the Thomson distribution. The same value of sputtered atoms energy is used in [14] for simulation of the high-energy deposition of titanium dioxide films. Since the tilt angle essentially depends on the deposition angle, its divergence is not taken into account to demonstrate the formation of the chevron-like structure more clearly.

The inserted atoms that reflect from the substrate are removed from the simulation box after each injection step. The periodic boundary conditions are then applied. In each injection step, the *NVT* (constant number of particles, volume and temperature) ensemble is used. The vertical dimension of the simulation box is increased by 0.01 nm after each injection step in order to compensate for the growth of film thickness; the horizontal dimensions of the box remain unchanged.

The Berendsen thermostat [22] is applied to keep the simulation cluster temperature, $T = 300$ K, constant. The duration of one injection step is 6 ps and the time step of MD modeling is 0.5 fs. The maximum value of deposited film thicknesses is about 40 nm. MD simulation is performed using the GROMACS package [23] and visual analysis of the atomistic structures using the Visual Molecular Dynamic (VMD) [24] package.

The initial values of the deposited Si atoms' velocities are specified as follows (see also Figure 1):

$$v_z = v_0 \cos \alpha; v_x = v_0 \sin \alpha \sin \beta; v_y = v_0 \sin \alpha \cos \beta \quad (1)$$

where $\alpha = 80^\circ$ is the deposition angle, v_0 corresponds to the initial kinetic energy 10 eV of Si atoms, $\beta = \pm 90^\circ$ for the case of angle alternation and $\beta = \omega t + 90^\circ$ for the case of the continuous rotation, ω is rotation speed, $[\omega] = \text{rev/min}$, and t is deposition time. The deposition angle alternation is considered as the periodical variation of the deposition angle sign (see the left part of Figure 1). This alternation is treated as a step-wise substrate rotation under the condition that rotation time is much less than the time interval between subsequent alternations.

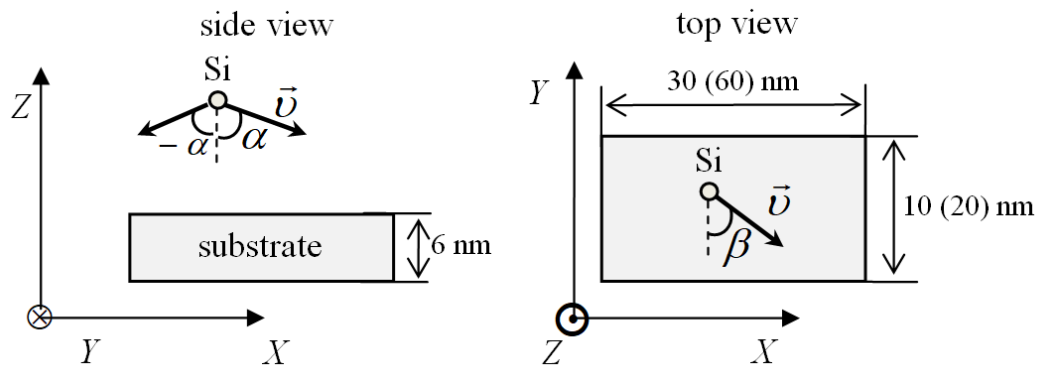


Figure 1. Schematic representation of the simulation area.

The simulation was carried out using equipment at the shared research facilities of high performance computing resources at Lomonosov Moscow State University [25].

3. Results and Discussion

The shape of the growing structures depends on the relationship between the deposition rate and rotation speed ω in the case of continuous rotation and on the time interval between subsequent alternations in the case of step-wise rotation [26]. If the deposition direction varies slowly compared to the deposition rate, helical or two-fold chevron structures grow on the substrate [26]. The opposite case corresponds to fast substrate rotation or fast alternation and results in the growth of vertical columnar structures [27]. These two regimes can be described using the following dimensionless parameter:

$$\varepsilon = r\tau/L \quad (2)$$

where r is the deposition rate, τ is the time interval between subsequent alternations and $\tau = 1/\omega$ in the case of continuous rotation, L is the average value of the horizontal dimension of the growing sculptured structure. In fact, the numerator in Equation (2) is the vertical thickness of the film, deposited during the time interval corresponding to one rotation or one deposition angle alternation. In the following, we assume that small values of ε correspond to fast rotation or alternation, large values of ε correspond to slow rotation or alternation and $\varepsilon \approx 1$ sets the boundary between these two regimes.

In the atomistic simulation of the GLAD process, it is convenient to define the value of ε in terms of the number of injection steps (see Section 2). Let h_1 , t_1 and n be the thickness of layer deposited per cycle, the duration of one cycle, and the number of injection steps between subsequent deposition angle alternations. Then $r = h_1/t_1$ and $\tau = t_1 n$. As was revealed in earlier simulations [19], approximately 3000 injection steps are enough to obtain a film with thickness of about 30 nm. On the other hand, the average thickness of the slanted columns forming in the GLAD process is about 5 nm [19]. Substituting these values in Equation (2), we obtain:

$$\varepsilon = n/500 \quad (3)$$

Thus, $\varepsilon \approx 1$ if the number of the injection steps between subsequent alternations is about 500.

Results of the GLAD simulation with alternation of the deposition angle are presented in Figures 2 and 3. In accordance with the estimations presented above, the values of n from 100 to 300 correspond to the case of fast alternation. As is seen in Figures 2 and 3, in this case, vertical tree-like columns are

formed. Horizontal dimensions of these columns are close to those obtained earlier in simulation of GLAD without angle alternation [19].

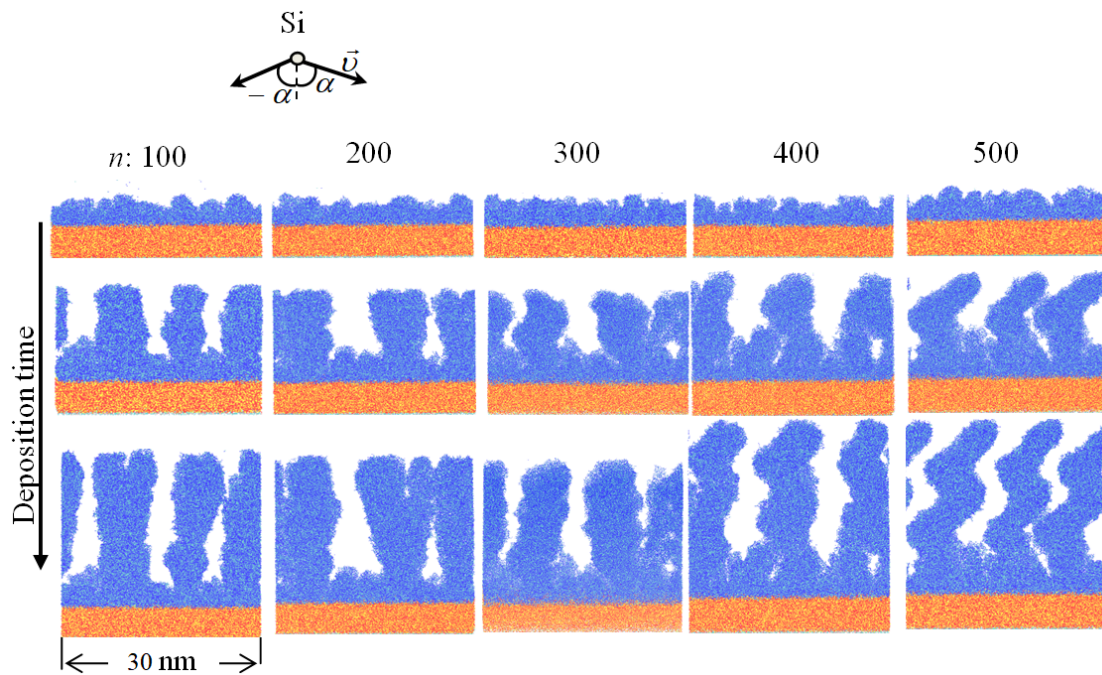


Figure 2. Atomistic structures of growing GLAD films on small substrates: side view in the X-Z plane. The deposition angle $\alpha = 80^\circ$ is altered after every n injection step. Energy of the deposited Si atoms is 10 eV. Substrate atoms are painted as yellow (Si) and red (O), deposited atoms are painted as green (Si) and blue (O).

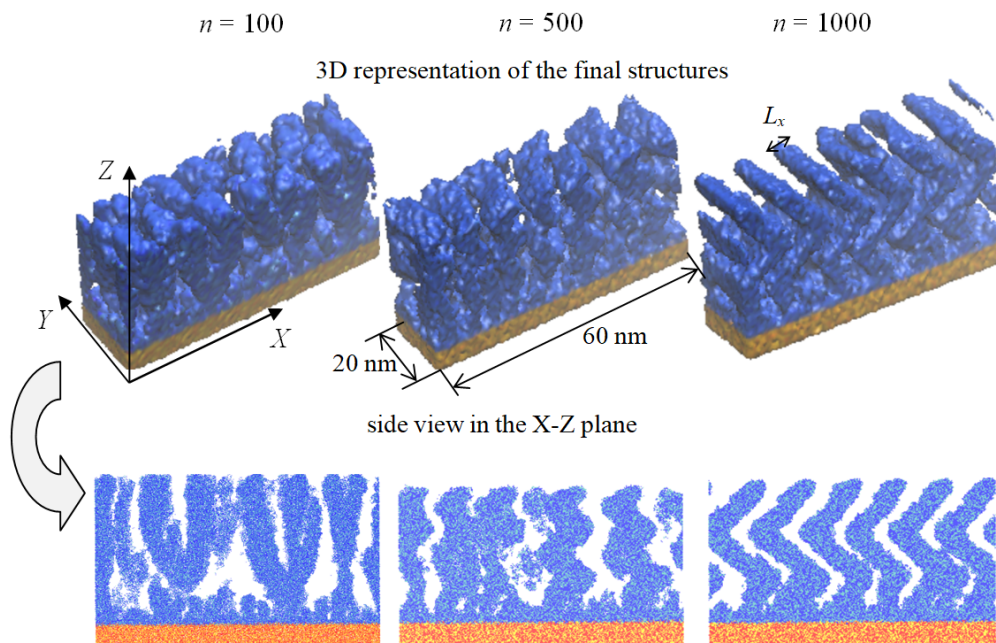


Figure 3. 3D representation of the final GLAD structures deposited on large substrates and side views in the X-Z plane. Other designations are the same as in Figure 2.

Deposition with $n = 400$ results in the formation of an intermediate structure between the tree-like and chevron-like structures. The increase of n to 500 results in a clearly visible regular two-fold chevron vertical structure.

3D views of final film clusters deposited on large substrates are shown in Figure 3. Side views in the X-Z plane complement 3D views in order to clearly demonstrate tree-like and chevron-like structures. The increase of n from 500 to 1000 results in more pronounced similarity of the growing film structure to the set of chevrons. The vertical step of these chevrons is about 20 nm (right part in Figure 3), which is about three times more than their thickness $L_x \approx 6$ nm in the X direction.

To calculate the density profiles (Figure 4), the final atomistic cluster is divided into horizontal layers with thickness $\Delta z = 1$ nm. The density ρ of each layer is calculated as follows:

$$\rho = N\mu/(N_a S \Delta z) \quad (4)$$

where N_a is Avogadro number, N is the number of SiO₂ groups in the considered layer, $\mu = 60$ g/mol is the molar weight of the SiO₂, S is the surface area of the considered cluster ($S = 300$ nm² and $S = 1200$ nm² for the small and large substrate clusters, respectively). All values are substituted in Equation (4) using the International System of Units.

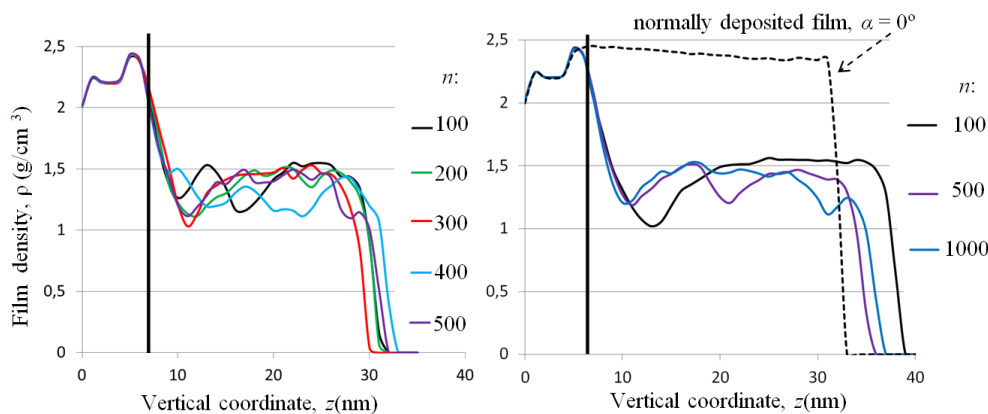


Figure 4. Density profiles of the films deposited on small substrate (left) and large substrate (right). Atomistic structures are shown in Figures 2 and 3. Energy of deposited Si atoms is 10 eV, deposition angle $\alpha = 80^\circ$, n is the number of injection steps between subsequent alternations of α . Vertical black line denotes the substrate boundary before the deposition.

Unlike the density profile of normally deposited film (dotted black curve at the right part of Figure 4), the GLAD films' density profiles vary noticeably with the growth of vertical coordinate z . We assume that the density decrease at the beginning of film deposition relates to the initial stage of the tree-like structure growth. Further density irregularities are due to irregularities of the simulated structures (see Figure 3). The thicknesses of the transition layers between substrate and film is about 10 nm, which exceeds the thicknesses of the transition layers between film and air.

Density values, averaged over the interval from $z = 10$ nm to $z = 30$ nm, where z is the vertical coordinate, are presented in Table 1. In all cases, the densities of GLAD films are essentially lower than the density of the normally deposited film—2.4 (g/cm³) [19]. Basing on the relationship between film density and refractive index [28], the value of refractive index in the case of GLAD films is estimated as 1.3, which is close to the published experimental value [29].

Table 1. Density ρ (g/cm³) of films deposited on the small and large substrate clusters (Figures 2 and 3); n is the number of injection steps between subsequent alternations of the deposition angle.

Subst. Dimens.	10 nm × 30 nm					20 nm × 60 nm		
n	100	200	300	400	500	100	500	1000
ρ	1.31	1.34	1.39	1.26	1.44	1.33	1.32	1.35

In our simulations, no regular dependence of ρ on the number of injection steps n has been revealed. Density profiles fluctuate around their average values. We suppose that these fluctuations are connected with the relatively small volumes of the deposited clusters. The reduction of fluctuations with the growth of substrate dimensions from $10 \text{ nm} \times 30 \text{ nm}$ to $20 \text{ nm} \times 60 \text{ nm}$ confirms this supposition.

The case of continuous substrate rotation has been also investigated. As in the case of GLAD with altering deposition angles, the shape of the growing structure essentially depends on the rotation speed [27]. In the presented work, the case of slow continuous rotation is considered. The rotation speed ω is specified, such that one rotation takes $n = 2000$ deposition cycles.

The resulting structure is shown in Figure 5. In contrast to Figures 2 and 3, only a free volume of the deposited structure is shown in this figure while the film matter is considered as transparent. This method of visualization presents the cluster structure more clearly than the traditional one. As expected, the slow rotation results in the formation of a helical structure. Because of the small size of the substrate (15 nm for both horizontal dimensions), only one helix is obtained. The helix makes approximately one complete rotation in the horizontal plane accordingly to the specified value of ω . The investigation of helical structures in more detail requires simulations with clusters of larger dimensions and can be performed in future when the practical potential of such structures become more evident.

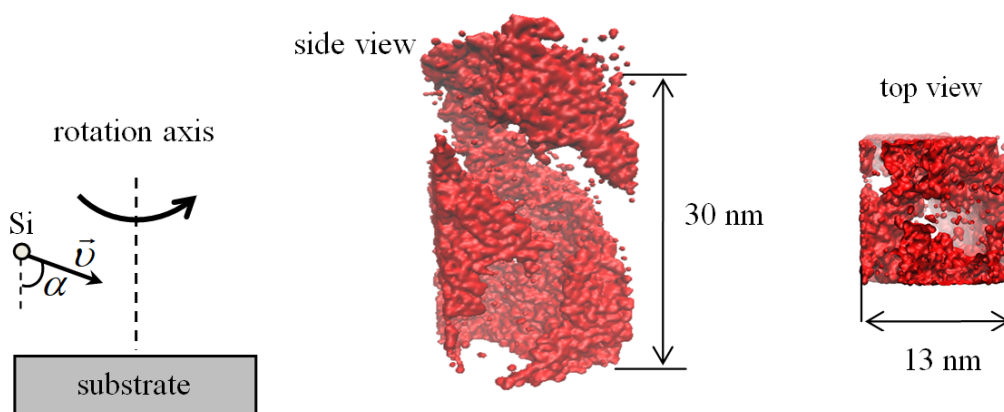


Figure 5. The helical structure growing under slow substrate rotation speed. The free volume inside the deposited films is painted in red.

4. Conclusions

The atomistic simulation of SiO_2 GLAD films with alternation of the deposition angle is carried out in this paper. The energy of the deposited Si atom is 10 eV and deposition angle is 80° . Based on the introduced dimensionless criteria, cases of slow and fast alternation are investigated separately. In accordance with the existing experimental data, it has been found that slow alternation results in the growth of vertical tree-like columns, while fast alternation leads to the formation of chevron-like regular structures with vertical step of about 20 nm. The densities of deposited films vary in the interval $1.3 \div 1.4 \text{ g/cm}^3$, which corresponds to the reduction of the refractive index to 1.3. The case of slow continuous rotation with the same deposition angle, 80° , is studied. The formation of the helical structure is also demonstrated. These results are in accordance with known experimental data. As a whole, the presented results demonstrate that at the current level of mathematical modeling, atomistic simulation of the deposition process becomes a reliable tool to predict thin film structural properties, depending on various parameters of the process.

Author Contributions: Conceptualization, A.V.T.; Investigation, F.V.G.; Supervision, V.B.S.; Writing – original draft, F.V.G.; Writing – review & editing, V.B.S. and A.V.T.

Funding: The work was supported by the Russian Science Foundation (grant number 19-11-00053).

Conflicts of Interest: The authors declare no conflict of interest.

References

1. Robbie, K.; Brett, M.J.; Lakhtakia, A. Chiral sculptured thin films. *Nature* **1996**, *384*, 616. [[CrossRef](#)]
2. Hawkeye, M.M.; Brett, M.J. Glancing angle deposition: fabrication, properties, and applications of micro- and nanostructured thin films. *J. Vac. Sci. Technol.* **2007**, *25*, 1317–1335. [[CrossRef](#)]
3. Woo, S.-H.; Park, Y.J.; Chang, D.H.; Sobahan, K.M.A.; Hwangbo, C.K. Wideband antireflection coatings of porous MgF₂ films by using glancing angle deposition. *J. Korean Phys. Soc.* **2007**, *51*, 1501–1506. [[CrossRef](#)]
4. Tkachenko, V.; Marino, A.; Otón, E.; Bennis, N.; Otón, J.M. Morphology of SiO₂ films as a key factor in alignment of liquid crystals with negative dielectric anisotropy. *Beilstein J. Nanotechnol.* **2016**, *7*, 1743–1748. [[CrossRef](#)]
5. Trottier-Lapointe, W.; Zabeida, O.; Schmitt, T.; Martinu, L. Ultralow refractive index optical films with enhanced mechanical performance obtained by hybrid glancing angle deposition. *Appl. Opt.* **2016**, *55*, 8796–8805. [[CrossRef](#)]
6. Tolenis, T.; Grinevičiūtė, L.; Buzelis, R.; Smalakys, L.; Pupka, E.; Melnikas, S.; Selskis, A.; Drazdys, R.; Melninkaitis, A. Sculptured anti-reflection coatings for high power lasers. *Opt. Mater. Express* **2017**, *7*, 1249–1258. [[CrossRef](#)]
7. Oliver, J.B.; Kessler, T.J.; Smith, C.; Taylor, B.; Gruschow, V.; Hettrick, J.; Charles, B. Electron-beam-deposited distributed polarization rotator for high-power laser applications. *Opt. Express* **2014**, *22*, 23883–23896. [[CrossRef](#)]
8. Oliver, J.B.; Smith, C.; Spaulding, J.; Rigatti, A.L.; Charles, B.; Papernov, S.; Taylor, B.; Foster, J.; Carr, C.W.; Luthi, R.; et al. Glancing-angle-deposited magnesium oxide films for high-fluence applications. *Opt. Mater. Express* **2016**, *6*, 2291–2303. [[CrossRef](#)]
9. Karabacak, T.; Singh, J.P.; Zhao, Y.P.; Wang, G.C.; Lu, T.M. Scaling during shadowing growth of isolated nanocolumns. *Phys. Rev. B* **2003**, *68*, 125408. [[CrossRef](#)]
10. Robbie, K.; Brett, M.J.; Lakhtakia, A. First thin-film realization of a helicoidal bianisotropic medium. *J. Vac. Sci. Technol. A* **1995**, *13*, 2991–2993. [[CrossRef](#)]
11. Smy, T.; Vick, D.; Brett, M.J.; Dew, S.K.; Wu, A.T.; Sit, J.C.; Harris, K.D. Three-dimensional simulation of film microstructure produced by glancing angle deposition. *J. Vac. Sci. Technol. A* **2000**, *18*, 2507–2512. [[CrossRef](#)]
12. Grüner, C.; Liedtke, S.; Bauer, J.; Mayr, S.G.; Rauschenbach, B. Morphology of Thin Films Formed by Oblique Physical Vapor Deposition. *ACS Appl. Nano Mat.* **2018**, *1*, 1370–1376. [[CrossRef](#)]
13. Backholm, M.; Foss, M.; Nordlund, K. Roughness of glancing angle deposited titanium thin films: an experimental and computational study. *Nanotechnology* **2012**, *23*, 385708. [[CrossRef](#)]
14. Badorreck, H.; Steinecke, M.; Jensen, L.; Ristau, D.; Jupé, M.; Müller, J.; Tonneau, R.; Moskovkin, P.; Lucas, S.; Pflug, A.; et al. Correlation of structural and optical properties using virtual materials analysis. *Opt. Express* **2019**, *27*, 22209–22225. [[CrossRef](#)]
15. Schmidt, D.; Schubert, M. Anisotropic bruggeman effective medium approaches for slanted columnar thin films. *J. Appl. Phys.* **2013**, *114*, 083510. [[CrossRef](#)]
16. Grigoriev, F.V.; Sulimov, A.V.; Katkova, E.V.; Kochikov, I.V.; Kondakova, O.A.; Sulimov, V.B.; Tikhonravov, A.V. computational experiments on atomistic modeling of thin film deposition. *Appl. Opt.* **2017**, *56*, C87–C90. [[CrossRef](#)]
17. Grigoriev, F.V.; Sulimov, A.V.; Katkova, E.V.; Kochikov, I.V.; Kondakova, O.A.; Sulimov, V.B.; Tikhonravov, A.V. Full-atomistic nanoscale modeling of the ion beam sputtering deposition of SiO₂ thin films. *J. N. Cryst. Sol.* **2016**, *448*, 1–5. [[CrossRef](#)]
18. Grigoriev, F.V.; Sulimov, A.V.; Katkova, E.V.; Kochikov, I.V.; Kondakova, O.A.; Sulimov, V.B.; Tikhonravov, A.V. Annealing of deposited SiO₂ thin films: full-atomistic simulation results. *Opt. Mater. Express* **2016**, *6*, 3960–3966. [[CrossRef](#)]
19. Grigoriev, F.V.; Sulimov, V.B.; Tikhonravov, A.V. Atomistic simulation of the glancing angle deposition of SiO₂ thin films. *J. N. Cryst. Sol.* **2019**, *512*, 98–102. [[CrossRef](#)]
20. Grigoriev, F.V.; Sulimov, A.V.; Kochikov, I.V.; Kondakova, O.A.; Sulimov, V.B.; Tikhonravov, A.V. Supercomputer modeling of the ion beam sputtering process: full-atomistic level. In Proceedings of the SPIE—The International Society for Optical Engineering, Jena, Germany, 21–24 September 2015; Volume 9627, pp. 962708-1–962708-9. [[CrossRef](#)]
21. Thompson, M.V. Atomic collision cascades in solids. *Vacuum* **2002**, *66*, 99–114. [[CrossRef](#)]

22. Berendsen, H.J.C.; Postma, J.P.M.; van Gunsteren, W.F.; DiNola, A.; Haak, J.R. Molecular-dynamics with coupling to an external bath. *J. Chem. Phys.* **1984**, *81*, 3684–3690. [[CrossRef](#)]
23. Abraham, M.J.; Murtola, T.; Schulz, R.; Páll, S.; Smith, J.C.; Hess, B.; Lindahl, E. GROMACS: High performance molecular simulations through multi-level parallelism from laptops to supercomputers. *SoftwareX* **2015**, *1–2*, 19–25. [[CrossRef](#)]
24. Humphrey, W.; Dalke, A.; Schulten, K. VMD: Visual molecular dynamics. *J. Mol. Graph.* **1996**, *14*, 33–38. [[CrossRef](#)]
25. Voevodin, V.I.; Antonov, A.; Nikitenko, D.; Shvets, P.; Sobolev, S.; Sidorov, I.; Stefanov, K.; Voevodin, V.V.; Zhumatiy, S. Supercomputer lomonosov-2: large scale, deep monitoring and fine analytics for the user community. *Supercomput. Front. Innov.* **2019**, *6*, 4–11. [[CrossRef](#)]
26. Lakhtakia, A.; Mesier, R. *Sculptured thin Films: Nanoengineered Morphology and Optics*; SPIE: Bellingham, WA, USA, 2005.
27. Christian, P.; Glancing Angle Deposition of Silicon Nanostructures by on Beam Sputtering. Universität Leipzig, Dissertation. Available online: https://www.iom-leipzig.de/fileadmin/redaktion/pdf/Dissertationen/Diss_Patzig_200dpi_sicher.pdf (accessed on 5 August 2019).
28. Vedam, K.; Limsuwan, P. Piezo- and elasto-optic properties of liquids under high pressure. II. Refractive index vs. density. *J. Chem. Phys.* **1978**, *69*, 4772–4778. [[CrossRef](#)]
29. Melninkaitis, A.; Grinevičiūtė, L.; Abromavičius, G.; Mažulė, L.; Smalakys, L.; Pupka, E.; Ščiuka, M.; Buzelis, R.; Kičas, S.; Tolenis, T. Next-generation allsilica coatings for UV applications. In Proceedings of the SPIE 10447, Laser-Induced Damage in Optical Materials, Boulder, CO, USA, 24–27 September 2017. 104470U. [[CrossRef](#)]



© 2019 by the authors. Licensee MDPI, Basel, Switzerland. This article is an open access article distributed under the terms and conditions of the Creative Commons Attribution (CC BY) license (<http://creativecommons.org/licenses/by/4.0/>).